Viscous Dissipation in Die Flows

The flow of polymer melts in cylindrical, annular, and slit dies has been examined. Large temperature rises at the outer surface of the extrudate were measured with an infrared pyrometer. Calculations show that severe radial temperature gradients exist in these flow geometries under conditions similar to those encountered in polymer processing and in viscometry measurements. A common method of estimating the average temperature rise from the total mechanical energy input seriously underestimates the maximum temperature rise.

A numerical solution of the flow and energy equations models the flow in all three geometries. A very simple Nusselt number correlation allowed an estimate of the temperature rises possible if heat transfer with the die wall occurs. Good agreement was obtained between predicted and infrared measured melt surface temperature rises. The pressure drop gives only an indication that nonisothermal flow is occurring and is not sensitive enough to distinguish the type of heat transfer boundary condition present.

The mathematical model presented could be helpful in die design and in process modeling, allowing the designer to obtain some knowledge of the kind of flow situations which might be encountered.

HOWARD W. COX
and
CHRISTOPHER W. MACOSKO

Department of Chemical Engineering and Materials Science
University of Minnesota
Minneapolis, Minnesota 55455

SCOPE

The internal heat generation caused by the shearing of fluid layers can greatly complicate attempts to model the flow of polymer melts through dies. Large temperature rises can occur in the regions of high shear rate near the walls of capillaries and dies. Significant flow rearrangement can occur due to the large temperature dependence of viscosity of most polymer melts. It is also possible that both chemical and mechanical degradation can occur due to the high temperatures and high shear rates.

The heat generation due to viscous dissipation is important in industrial processing of polymers. Large amounts of polymers are processed under conditions where shear heating undoubtedly exists. Very high shear rates can occur in the nozzles of injection molding machines, resulting in significant temperature rises. Shear heating can also play an important role in the extrusion of polymeric materials. In fact, a significant portion of the heat necessary to bring the polymer melt up to the processing temperature in a plasticating extruder is furnished by the shearing of the polymer.

The flow of polymer melts in cylindrical, annular, and slit dies has been examined. The surface temperature of the melt extrudate was determined at different flow rates by an infrared pyrometer. The technique of using infrared pyrometry to measure surface temperatures of plastics is relatively new. It provides a noncontact method of obtaining temperature rises without disturbing the flow. An attempt has been made to simulate the data with a numerical solution of a mathematical model.

CONCLUSIONS AND SIGNIFICANCE

Fairly large temperature rises, up to 70°C, have been observed for the flow of polymer melts in three die geometries. Calculations show that severe radial temperature gradients exist in these flow geometries under conditions similar to those encountered in polymer processing and in viscometry measurements. A common method of estimating the average temperature rise from the total mechanical energy input is quite inadequate in predicting the maximum temperature rise.

A numerical solution of the flow equations models the flow situation in all three geometries. A very simple Nusselt number correlation gives good agreement between predicted and infrared measured melt surface temperature rises. The pressure drop gives only an indication that nonisothermal flow is occurring and is not sensitive enough to distinguish the type of heat transfer boundary condition present. The assumption of incompressibility was examined and appears valid.

PREVIOUS WORK

Brinkman (1951) considered shear heating in the flow of a Newtonian fluid with constant physical properties. Bird (1955) obtained an analytical solution for the flow of a non-Newtonian fluid also with constant physical properties. Toor (1956, 1957) included the effect of cooling resulting from expansion during flow.

Gee and Lyon (1957) obtained a numerical solution for the situation with temperature dependent viscosity but presented little data with which to evaluate their assumptions, such as the assumption of an isothermal wall.

Correspondence concerning this paper should be addressed to C. W. Macosko. H. W. Cox is with General Motors Research Laboratories, Warren, Michigan 48090.

Gerrard et al. (1965, 1966) have presented a detailed analysis of a Newtonian oil. They include radial flow and pressure dependence of the viscosity in their numerical solution. Their experimental measures of flow rate and temperature profile are in good agreement with their calculated results. They found that an adiabatic wall best described the actual situation.

Morrette and Gogos (1968) have considered the flow of a rigid polyvinyl chloride and attempted to account for the effects of thermal degradation. Their theoretical results do not agree very well with their experimental data.

Galili and Taskerman-Krozer (1971) have presented an analytical solution using a perturbation method and assuming a Newtonian fluid with temperature dependent viscosity. They were able to obtain a first-order approximation to the stream function and pressure distribution but only a zeroth order approximation to the temperature distribution (the Brinkman solution).

Previous investigators (Marshall, et al., 1964; Van Leeuwen, 1967; Kim and Collins, 1971) have attempted to make temperature measurements of the flowing melt using thermocouples. Their efforts have met with little success primarily due to the problem of shear heating on the thermocouple itself and the disruption of the flow field. Temperature sensitive paints and melting point compounds have also been tried (Macosko, 1970) but were found to be pressure sensitive or soluble in the melt.

There does not appear to be a complete solution for the non-Newtonian case in the literature (Porter, 1971). Experimental data is particularly lacking.

MATHEMATICAL MODEL

Nonisothermal flow problems require the solutions to the coupled equations of continuity, momentum, and energy. The governing equations for flow between two parallel plates (an infinitely wide rectangle or slit) will be presented. The solution to the problem of flow in cylindrical and annular conduits can be obtained in a similar manner by making the necessary modifications to the equations of change and the governing boundary conditions.

The separation between the plates is of a distance d, with the width of the area for flow being a distance b. The length of the plates is L. A coordinate system is established at the midplane, $d/2$, between the plates such that z is the principal direction of flow, y is the thickness coordinate, and x is the width coordinate. It has been assumed the aspect ratio b/d is sufficiently large such that there is no x dependence and a two-dimensional problem exists. Other assumptions include:

1. Laminar steady flow
2. Symmetry about the z axis
3. No fluid slip at the wall
4. Negligible heat transfer by conduction in the z direction (as compared with convection)
5. The pressure is uniform in the y direction
6. Negligible inertial effects in the momentum equation
7. Negligible normal stresses—those due to acceleration as well as elasticity
8. Thermal conductivity k, and heat capacity c_p are independent of temperature and pressure but the density can be expressed by an equation of state $\rho = \rho(T, P)$.
9. The viscosity can be expressed as $\eta = \eta(\dot{\gamma}, T, P)$ where the shear rate $\dot{\gamma}$ is the magnitude of the velocity gradient perpendicular to the direction of flow, $\frac{\partial v_z}{\partial y}$ and the shear stress can be written as $\tau = -\eta \frac{\partial v_z}{\partial y}$.

With these assumptions, the equations of change in rectangular coordinates reduce to

$$\frac{\partial}{\partial z}(\rho v_z) + \frac{\partial}{\partial y}(\rho v_y) = 0 \tag{1}$$

$$0 = -\frac{dP}{dz} - \frac{\partial \tau_{yz}}{\partial y} \tag{2}$$

$$\rho c_p \left(v_z \frac{\partial T}{\partial z} + v_y \frac{\partial T}{\partial y} \right) = k \frac{\partial^2 T}{\partial y^2} - \tau_{yz} \frac{\partial v_z}{\partial y} + T\epsilon v_z \frac{dP}{dz} \tag{3}$$

The second term on the right side of Equation (3) is the viscous heat generation term while the last term accounts for the effect of expansion during flow, where ϵ is the coefficient of thermal expansion $-\frac{1}{\rho}\left(\frac{\partial \rho}{\partial T}\right)_P$. As a compressible fluid flows down a conduit, it expands due to the decreasing pressure, absorbing energy as it expands. Toor (1956) gives an excellent discussion as to how this term arises in the energy equation.

The applicable boundary conditions are

$$\frac{\partial T}{\partial y} = 0 \qquad y = 0, \quad 0 < z < L$$

$$\tau_{yz} = 0 \qquad y = 0, \quad 0 < z < L$$

$$v_z = v_y = 0 \qquad y = d/2, \quad 0 < z < L$$

$$-k\frac{\partial T}{\partial y} = h(T - T_0) \qquad y = d/2, \quad 0 < z < L$$

$$P = 0 \qquad z = L, \quad 0 < y < d/2$$

It has also been assumed that fully developed non-Newtonian isothermal flows exist at the entrance of the slit, that is,

$$T = T_0 \qquad z = 0, \quad 0 < y < d/2$$

$$v_z = v_{z0}(y) \qquad z = 0, \quad 0 < y < d/2$$

$$v_y = 0 \qquad z = 0, \quad 0 < y < d/2$$

where $v_{z0}(y)$ is the solution to Equation (2) at a temperature T_0.

It should be noted that a heat transfer coefficient at the wall is assumed. Most previous work assumed either an isothermal wall or an adiabatic wall. The data obtained for this study indicated that neither situation existed. The assumption of a heat transfer coefficient allows an estimate of the temperature rises occurring in the system without considering the more complicated problem of melt flow coupled with die conduction.

A better boundary condition at $y = d/2$ is

$$\left(-k\frac{\partial T}{\partial y}\right)_{\text{melt}} = \left(-k\frac{\partial T}{\partial y}\right)_{\text{die}}$$

This boundary condition requires knowledge of the temperature distribution in the die also. Ignoring axial conduction in the die results in an effective heat transfer coefficient which is independent of the melt flow rate, contrary to the data presented. Considering axial conduction requires solving Laplace's equation for the die subject to the above boundary condition and boundary conditions at $y = y_d > d/2$, $z = 0$ and $z = L$. The boundary conditions at $y = y_d$ and $z = L$ are very uncertain, and this uncertainty as well as the complexities of solving the coupled problems is sufficient to warrant simplification of the boundary condition to that used, namely,

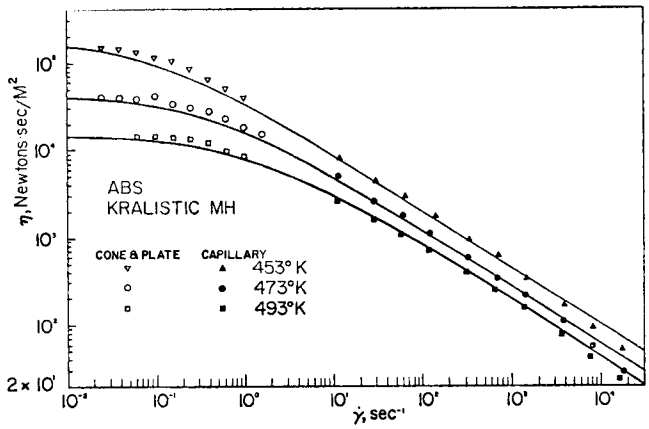

Fig. 1. Viscosity relationship and experimental viscometry data.

$$-k\frac{\partial T}{\partial y} = h(T - T_0) \quad y = d/2,\ 0 < z < L$$

The coupled nonlinear system of Equations (1 to 3) does not appear to have an analytical solution. A numerical solution by finite difference methods was obtained. The solution resembles that of Gerrard et al. (1965, 1966). Some of the details are in an appendix.

EXPERIMENT

Materials

The polymers used in this study were acrylonitrile butadiene styrene, ABS, (Cycolac T from Marbon and Kralastic MH from Uniroyal), and a branched polyethylene (DFDC 0506NT from Union Carbide).

Viscometry and Physical Properties

Viscosity data for one of the ABS materials (Kralastic MH) was taken over a wide range of shear rate. A Rheometrics Mechanical Spectrometer (Rheometrics, Inc.) in the cone and plate mode was used to gather the low shear rate data. Its operation is described elsewhere (Macosko and Starita, 1971). Data was obtained in the shear rate range of 0.025 sec^{-1} to 1.575 sec^{-1}. Both 25 mm and 50 mm plates were used with a cone of angle 0.04 radians. The samples were vacuum compression molded to prevent any entrapment of air (Rogers et al., 1968).

The capillary rheometer used for the high shear rate data was one built in our own laboratory and is similar to the standard Instron capillary rheometer as described Merz and Colwell (1958). A set of capillaries with a diameter of 0.0511 cm and length to diameter ratios of 4, 8, 12, and 30 was used to obtain the viscosity data. All capillaries had a flat 180° entrance. The apparent shear rate range obtained was 8.98-8980 sec^{-1}. The capillary data was corrected for entrance effects by a method described by Bagley (1957). Rabinowitsch corrections (Middleman, 1968) were applied to the shear rate to account for the non-Newtonian velocity profile of the polymer being tested. The standard isothermal and incompressible flow conditions were assumed. Details of the equipment and procedure are given by Cox (1973).

The viscosity relationship used is one reported by Bergen and Morris (1970) and is an adaptation of one derived from molecular considerations by Gillespie (1965).

$$\eta = \frac{\eta_0}{1 + c_1(\eta_0\dot{\gamma})^m} \tag{4}$$

This $\eta - \dot{\gamma}$ functionality is convenient to use as it has a Newtonian range at low shear rates and tends to a power law functionality at high shear rates.

The temperature dependence is assumed to be in the Newtonian viscosity in that

$$\eta_0(T) = \eta_0(T_r)a_T(T) \tag{5}$$

where T_r is a reference temperature. The temperature shift factor $a_T(T)$ is given by a WLF type of equation

$$\log a_T = -\frac{c_1(T - T_r)}{c_2 + (T - T_r)} \tag{6}$$

Viscosity data for the Kralastic material and the viscosity relation Equation (4) are compared in Figure 1. The values of the parameters for Equations (4) and (6) are listed in Table 1 along with other physical properties of the ABS. Some deviation between the function and the capillary data occurs at shear rates greater than 2000 sec^{-1} and at the lowest temperatures. Shear heating is undoubtedly present at these high shear rates. It is more predominant at the lower temperatures because the shear stress is greater at these temperatures. Shear heating has been shown to be an important factor in capillary viscometric studies (Cox and Macosko, 1974; Cox, 1973) and will not be discussed here.

Viscosity data for the other ABS material, Cycolac T, were taken with an Instron capillary rheometer as reported earlier (Cox and Macosko, 1974). The parameters for Cycolac T are also listed in Table 1.

It should be noted that the density of both ABS materials was assumed constant in the calculations as an equation of state was not readily available.

A viscosity function for the polyethylene used has been reported by Donovan (1971). It is an empirical function of temperature and shear rate fitted to capillary viscosity data. The form of the equation is

$$\ln\eta = a_1 + a_2\ln\dot{\gamma} + a_3(\ln\dot{\gamma})^2 + a_4T + a_5T^2 + a_6T\ln\gamma \tag{7}$$

with the values of the parameters given in Table 2 along with other physical properties of the branched polyethylene. An equation of state for the polyethylene melt was also reported by Donovan and is used in the calculations

$$\rho = a_7 + a_8T + a_9P \tag{8}$$

Table 1. ABS Physical Properties

Viscosity parameters for Equations (4) and (6)

	Kralastic MH (Uniroyal)	Cycolac T (Marbon)
$\eta_r = \eta_0$ at $T = Tr$, N · s/m²	4.46×10^4	1.32×10^4
T_r, °K	473	477.5
m	0.647	0.71
c_l, $(N/m^2)^{-m}$	1.80×10^{-3}	3.79×10^{-4}
c_1	3.46	3.96
c_2, °K	131	138

Data from Macosko (1970)

$\rho = 979$ kg/m³
$k = 0.279$ w/m °K
$c_p = 2.26 \times 10^3$ j/kg °K

Table 2. Polyethylene Parameters from Donovan (1971)

$\rho = 983 - 0.476\,T + 27.8\,P$
ρ in kg/m³
T in °K
P in N/m²
$k = 0.182$ w/m °K
$c_p = 2.60 \times 10^3$ j/kg °K

viscosity:

$$\ln\eta = a_1 + a_2\ln\dot{\gamma} + a_3(\ln\dot{\gamma}) + a_4T + a_5T^2 + a_6T\ln\dot{\gamma}$$

η in N s/m²
T in °K

$a_1 = 17.795$
$a_2 = -0.7771$
$a_3 = -1.946 \times 10^{-2}$
$a_4 = -2.539 \times 10^{-2}$
$a_5 = 1.36 \times 10^{-5}$
$a_6 = 7.92 \times 10^{-4}$

Temperature Measurement

With each flow geometry, an infrared pyrometer was focused on the melt extrudate right at the die exit. As the polymer was extruded, the melt surface temperature was measured by the pyrometer. Figure 2 shows schematically the arrangement of the infrared pyrometer.

The infrared pyrometer used was an Ircon Model CH-34L (Van Ness, 1965). The principle which the instrument uses is that all objects emit radiant energy and the intensity of this radiation is a function of its temperature. This particular device is filtered such that it senses radiation only in the range 3.36-3.50 microns. 3.43 microns is the center of the carbon-hydrogen bond absorption band common to nearly all polymers. Thus only the temperature close to the surface of materials exhibiting this absorption band will be measured by the Ircon. The temperature measurements are made by sensing the amount of infrared radiation the surface is emitting and converting this radiation intensity to a temperature by a calibrated indium antimonide detector. Field of view optics limit the sensed radiation to that coming from a specified area. The optics of the Ircon pyrometer with the Ircon M-2 lens permitted a circular area as small as 0.185 cm in diameter to be selected as the area of interest.

The Ircon measurements were verified by heating some molded ABS samples to several known temperatures and measuring their temperature with the infrared pyrometer. The emittance was set at 0.96, that of completely opaque (to infrared radiation) plastic. Accuracy of the instrument was

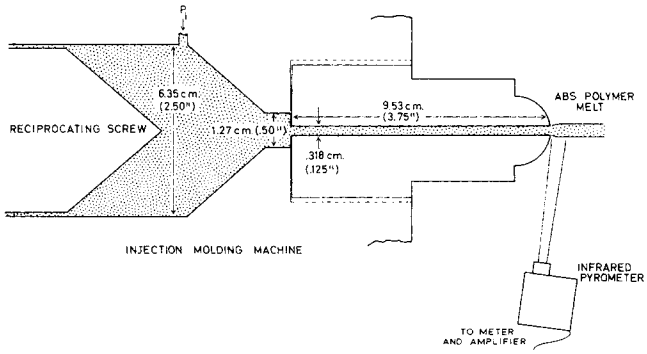

Fig. 2. Capillary flow with infrared surface temperature measurement.

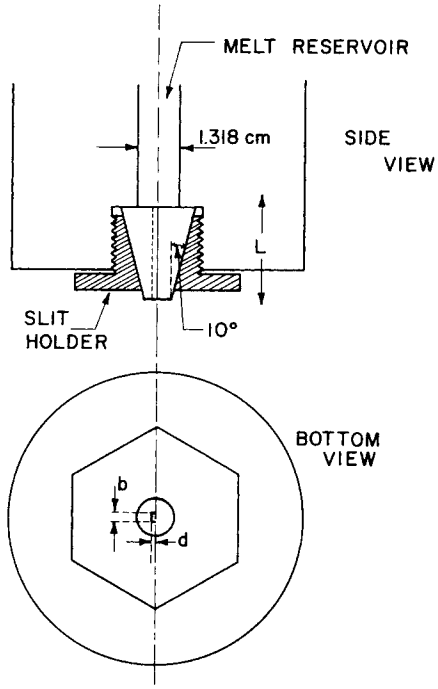

Fig. 3. Schematic of slit construction.

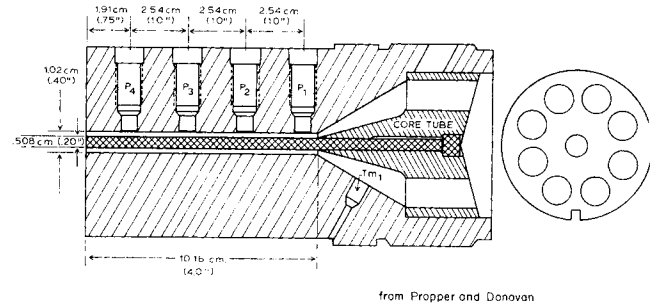

Fig. 4. Annular flow die.

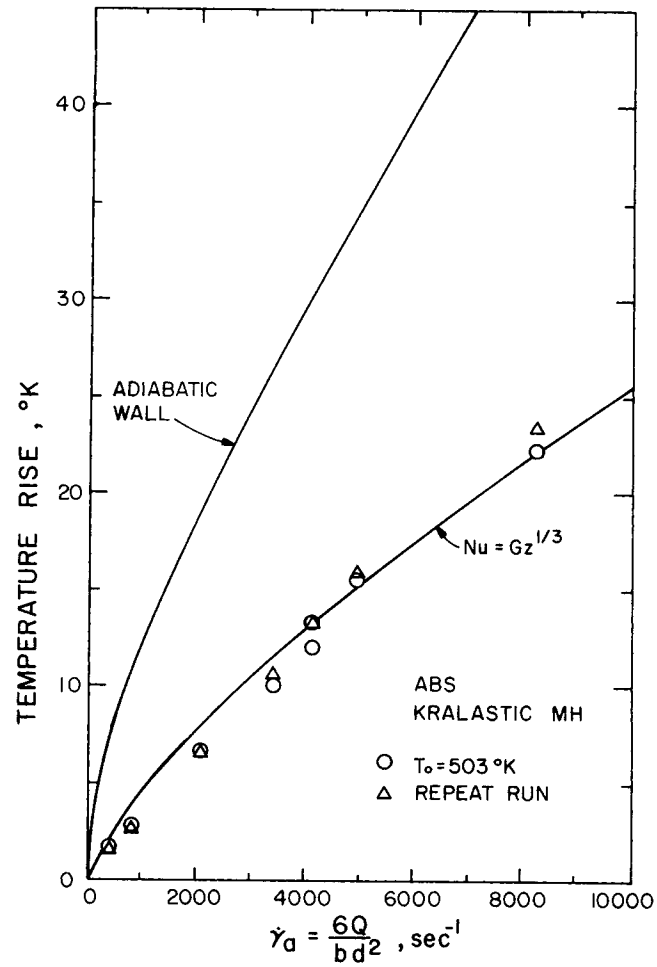

Fig. 5. Melt surface temperature rise—slit flow.

estimated to be ±3°K in measuring the magnitude of the temperature and ±1°K in determining temperature changes.

Slit Flow

Slit dies were inserted in the rheometer described earlier in place of the capillaries. The dies consisted of two conical stainless steel halves with a 10° taper which fit snugly into a matched stainless steel holder. The area for flow was machined into the flat side of one of the conical halves. The other conical piece was not machined and formed one of the walls of the flow area. The holder was threaded into the rheometer, holding the slit halves in place. A schematic of the slit rheometer is shown in Figure 3. The pressure of the polymer in the melt reservoir helped to seal the slit halves together. Leakage between the slit faces was very minimal. The dimensions of the slit used here are: depth $d = 0.0457$ cm, width $b = 0.4031$ cm, and length $L = 2.683$ cm. Two other slits were used by Cox (1973). One had a smaller depth but nearly the same b/d ratio while the other had a similar depth but a much larger

b/d ratio. The results are similar, but some effect of dimensions was observed and is discussed elsewhere (Cox, 1973).

Capillary Flow

For the capillary flow, a 0.318-cm diameter capillary 9.53 cm long was placed on the end of a reciprocating screw injection molding machine (see Figure 2). The ABS could be extruded or injected through this capillary over a wide range of flow rates. The flow rate was determined by cutting and weighing the extrudate. The pressure near the inlet of the capillary, P_i in Figure 2, was transmitted through a short tube of silicon grease to a Bourdon gauge.

Annular Flow

The annular flow experiment discussed here has been performed and reported by Propper and Donovan (1971). A schematic of their annulus is reprinted in Figure 4. They also used an Ircon infrared pyrometer to measure the surface temperature of the melt extrudate. The extrudate bulk temperature was recorded using a needle probe pyrometer.

RESULTS AND DISCUSSION

Slit Flow

The infrared measured surface temperature rises are shown in Figure 5. The solid lines are temperature rises calculated by the mathematical model presented earlier. There is a fairly large temperature rise occurring, but the assumption of an adiabatic wall ($Nu = 0$) predicts much too large a temperature rise. A very simple Nusselt number correlation was used as it allowed an estimate of the temperatures possible if neither an isothermal wall nor an adiabatic situation existed. This correlation does appear to give a reasonable estimate of the measured temperature rises.

The predicted and experimental pressure drops for the slit experiment are shown in Figure 6. The pressure drops have been adjusted for end effects using corrections obtained from the capillary viscosity data presented earlier. The flow appears to show some departure from isothermal flow at the higher shear rates, but the data does not seem to give any insight into the type of heat transfer boundary condition present.

Capillary Flow

The infrared measured wall temperature rises are shown in Figure 7. Again, there is a large rise, but an adiabatic wall predicts much too large a temperature rise. Calculations made with $Nu = Gz^{1/3}$ and $Nu = 1.75\ Gz^{1/3}$ are also shown and seem to give a more reasonable agreement.

Predicted and experimental reduced pressure drops are compared in Figure 8. The flow appears definitely nonisothermal. However, pressure drop measurements alone are not accurate enough to differentiate between the adiabatic flow curve and the flow curve with heat transfer. The measured pressure drops have not been corrected for end effects. However, since the capillary had an L/D ratio of 30, it is long enough for entrance effects to be minimal (Macosko, 1970).

A set of typical temperature and velocity profiles predicted for flow through the experimental capillary are shown in Figures 9 and 10. As can be seen from Figure 9, the temperature rise occurs in the region very near the wall with little or no temperature rise in the center of the die. The region near the wall is the region of high shear, and thus it is expected that this region have the largest temperature rise. It is interesting to note that the profile for $z/L = 0.201$ has a maximum temperature rise equal to 50% of the maximum temperature rise of the exit profile, $z/L = 1.0$. Thus, the region near the entrance of the die plays an important role in the development of the temperature profile. The bulk temperature rise is quite low compared to the maximum temperature rise occurring in the die. Caution should be exercised in using the bulk temperature rise for design purposes.

Figure 10 shows there is some rearrangement of the velocity profile as the exit profile ($z/L = 1.0$) is much flatter than the entrance profile. As the velocity profile becomes flatter, shear heating is enhanced by the steeper velocity gradient, resulting in even flatter velocity profiles. Shear heating is lessened, however, by a decrease in viscosity as the temperature rises, resulting in a smaller amount of heat generation. For incompressible flow, the velocity profile rearrangement seen in Figure 10 must be due to radial flow if continuity is to be satisfied.

Figure 11 is a plot of the predicted pressure profiles for this situation. There is some curvature of the profile which is caused by shear heating. It is more pronounced

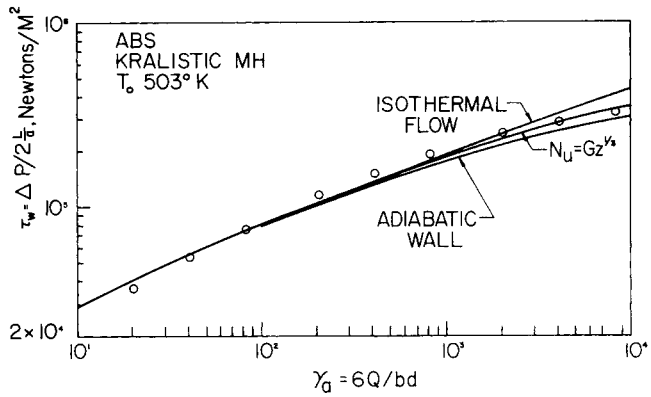

Fig. 6. Reduced pressure drop—slit flow.

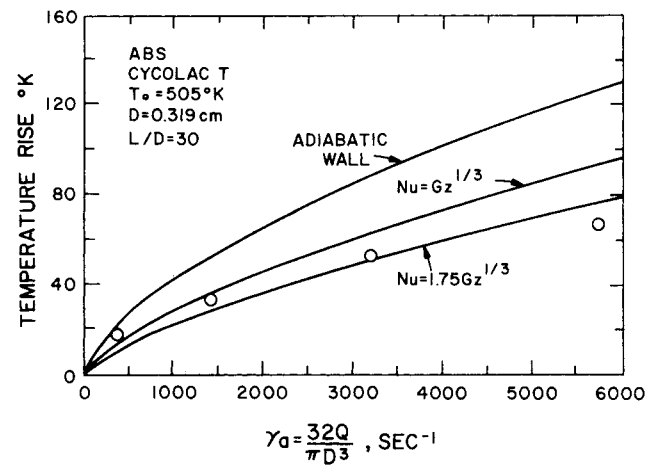

Fig. 7. Melt surface temperature rise—cylindrical flow.

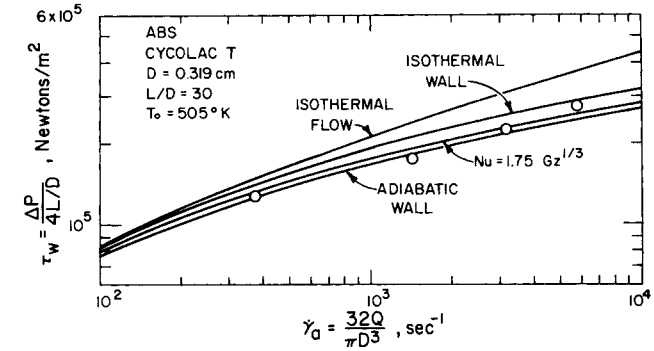

Fig. 8. Reduced pressure drop—cylindrical flow.

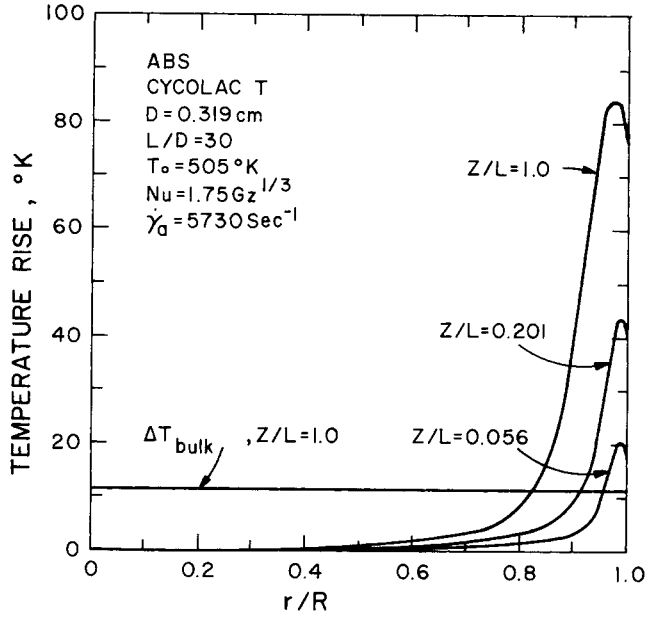

Fig. 9. Temperature profile—cylindrical flow.

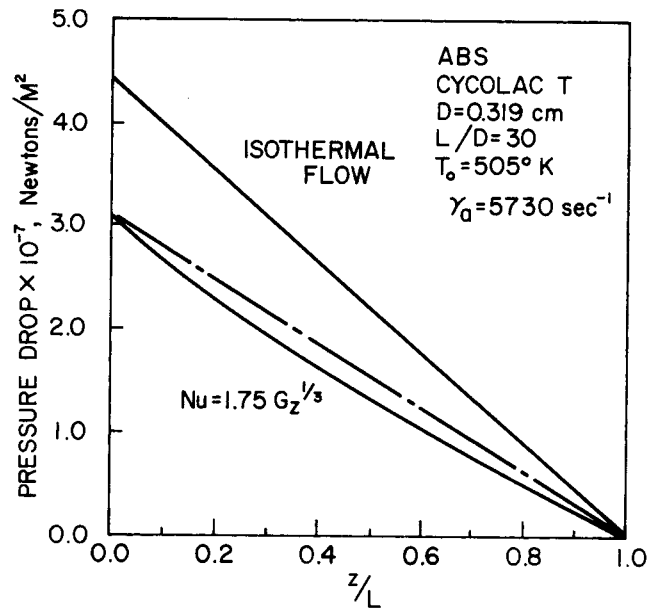

Fig. 11. Pressure profile—cylindrical flow.

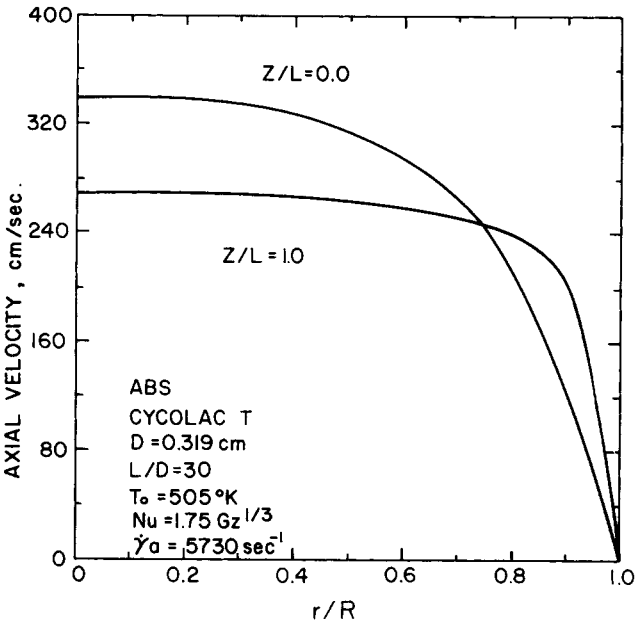

Fig. 10. Axial velocity profile—cylindrical flow.

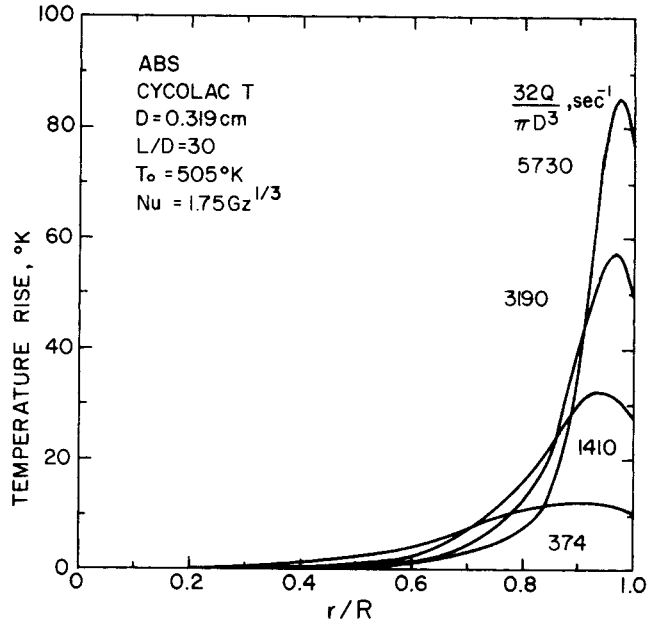

Fig. 12. Temperature profile at capillary exit.

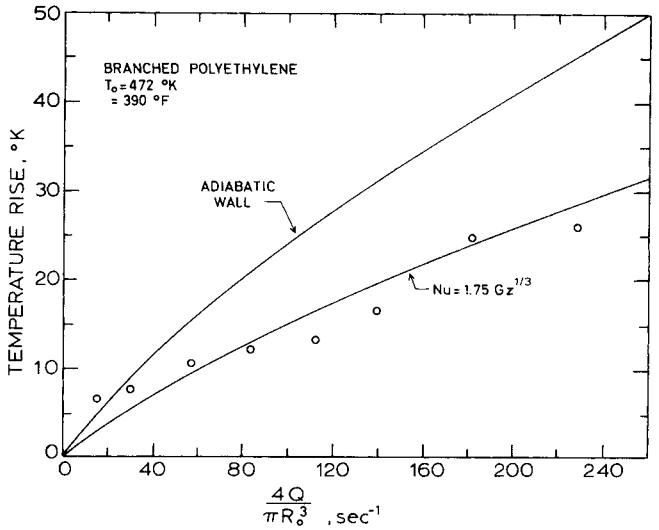

Fig. 13. Melt surface temperature rise—annular flow.

near the entrance of the die, the region which has the largest effect of shear heating. The isothermal flow profile is also shown for comparison. A 30% reduction in the pressure drop is seen as a result of shear heating.

Figure 12 shows the calculated temperature profiles at the exit of the die for different apparent shear rates. It shows quite clearly the effect of the flow rate on the heat generation and the temperature distribution. As the flow rate is increased, there is a larger temperature rise due to the increased heat generation but the temperature rise is confined to a smaller region near the wall. The larger flow rates allow less conduction of heat to the center of the die due to the shorter residence time.

Annular Flow

The infrared measured outer wall temperature rises reported by Propper and Donovan (1971) are shown in Figure 13. Also shown are the temperature rises predicted

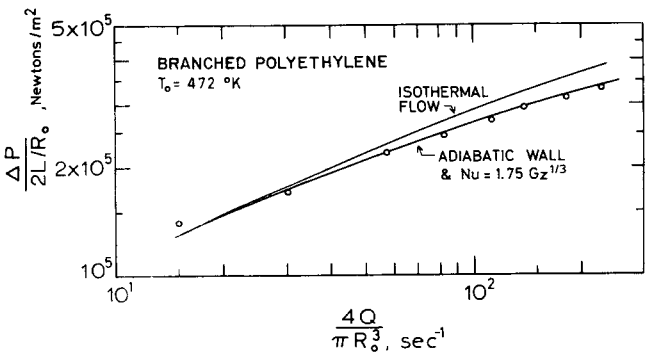

Fig. 14. Reduced pressure drop—annular flow.

by the model. Again, as with the other die geometries, adiabatic walls (inner and outer) predict too large a temperature rise. However, using the Nusselt number correlation, $Nu = 1.75\ Gz^{1/3}$, for the outer wall only (adiabatic inner wall), the predicted outer wall temperature rises agree rather well with the experimentally measured values.

An adiabatic inner wall was assumed as the surface area available for heat transfer is small. Any transferred energy could only be dissipated by conduction down the center rod and out the ends. Also, calculations show there is little effect of Nu_i on the outer wall temperature rise or pressure drop, the only experimentally available variables.

Figure 14 compares predicted and experimental reduced pressure drops. As in the other die geometries, pressure drop alone is not sensitive enough to distinguish between the adiabatic and heat transfer situation. In fact, as is shown, the theoretical curves superpose. The isothermal flow curve is presented for comparison.

Table 3 gives a comparison of the bulk temperature rises. A common method (Pearson, 1966) of estimating the average temperature rise from the total mechanical energy input can be shown to grossly underestimate the maximum temperature rise. If the flow were assumed to be adiabatic and incompressible, the maximum bulk temperature rise possible is given by

$$\Delta T_b = \frac{\Delta P}{\rho c_p} \tag{9}$$

As can be seen from Table 3, the measured temperature rise of the extrudate surface is much greater than the value determined by Equation (9) and the bulk temperature rise calculated by the mathematical model.

There appears to be some questions as to the accuracy of the experimentally measured bulk temperature rises. Values calculated using Equation (9) are less than those measured for the higher flow rates. It is possible that the large temperature gradients near the walls (see Figure 15) can cause erroneous measurements with a needle pyrometer. The probe diameter was approximately the annular gap so that the probe undoubtedly hits the hot inner surface of the annulus.

A typical set of temperature and velocity profiles is shown in Figures 15 and 16. As was seen with the other die geometries, almost all of the temperature rise occurs in the regions near the walls. The cooling effect of thermal expansion is clearly seen as there is a temperature drop in the center part of the annulus. As an equation of state was available for the polyethylene (see Table 2), the effect of compressibility and thermal expansion could be determined. The cooling effect is important only in the region away from the walls. Near the walls, shear heating is much larger than the cooling effect, which goes to zero at the wall.

Figure 16 shows that there is little rearrangement of the velocity profile due to shear heating. This is primarily due to the relatively low temperature dependence of viscosity for this polyethylene.

A comparison of calculated pressure profiles and experimental data is shown in Figure 17. There is much less curvature of the profiles than observed in the slit and capillary flow. Again, this can be explained partially by the relatively low temperature dependence of this polyethylene.

Figure 18 shows the predicted temperature profiles at the annulus exit over the flow rate range. It is interesting to note there is more cooling in the center of the annulus at the higher flow rates. This is due, of course, to the increased pressures necessary for the higher flow rates.

Calculations to test the significance of compressibility and expansion were made for $\frac{4Q}{\pi R_o^3} = 228\ \text{sec}^{-1}$ with the results summarized in Table 4. As can be readily seen, there is little effect on the temperature rise at the outer wall or the reduced pressure drop, variables for which experimental data exist. There is, however, a substantial lowering of the bulk temperature rise when the effect of expansion is considered. This is due to the cooling effect

Table 3. Bulk Temperature Rises

$\frac{4Q}{\pi R_0^3}$, s⁻¹	ΔT_b experimental	$\frac{\Delta P_{exp}}{\rho c_p}$	ΔT_b*	ΔT_{R0} experimental
15	2	2.84	2.63	7
57	4	4.45	4.39	11
83	6	5.01	4.99	12
139	10	5.96	5.86	17
182	10	6.34	6.34	25
228	12	6.83	6.75	26

Temperature rises in °K
$T_0 = 472$°K
*ΔT_b, calculated with both walls adiabatic
$\rho = \rho_0$, $\epsilon = 0$ (incompressible flow)

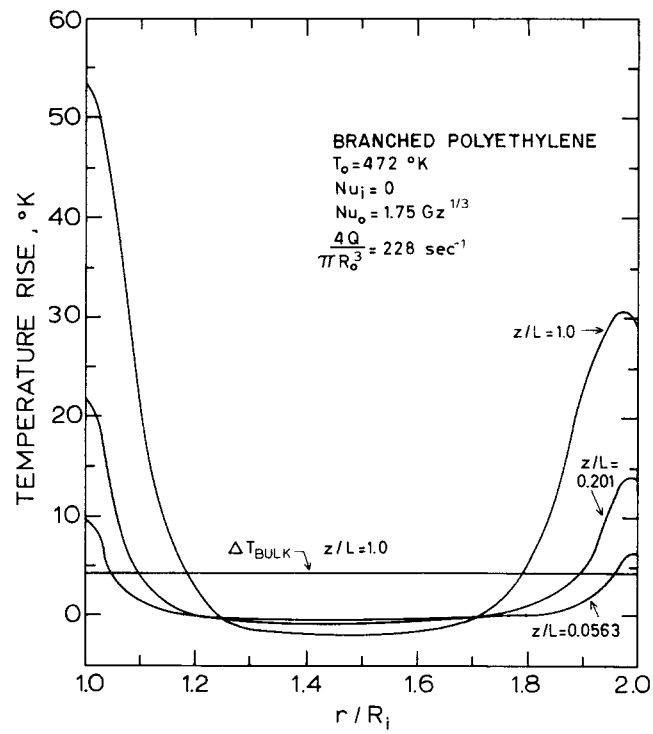

Fig. 15. Temperature profile—annual flow.

of the expansion of the melt during flow. However, there is no experimental data on the temperature in the middle of the die upon which to substantiate the importance of thermal expansion.

Pressure Dependence of Viscosity

All the calculations reported here have neglected the pressure dependence of viscosity. Some representative

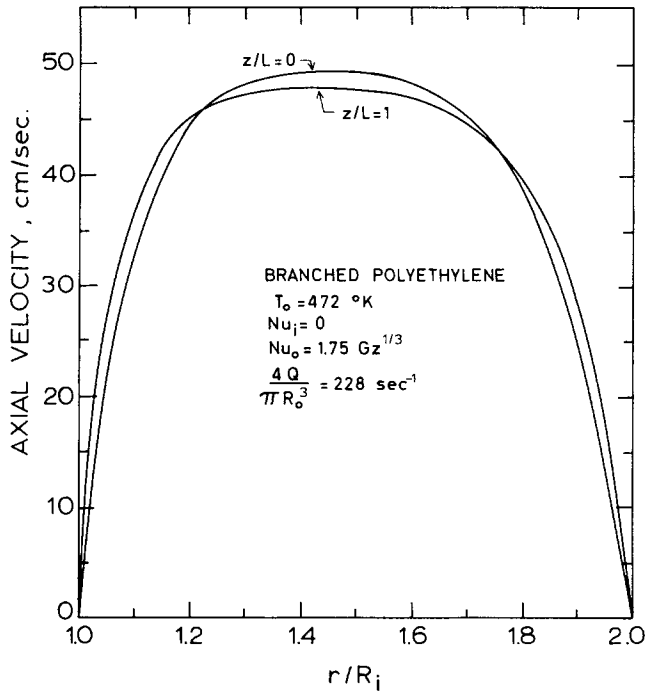

Fig. 16. Axial velocity profile—annular flow.

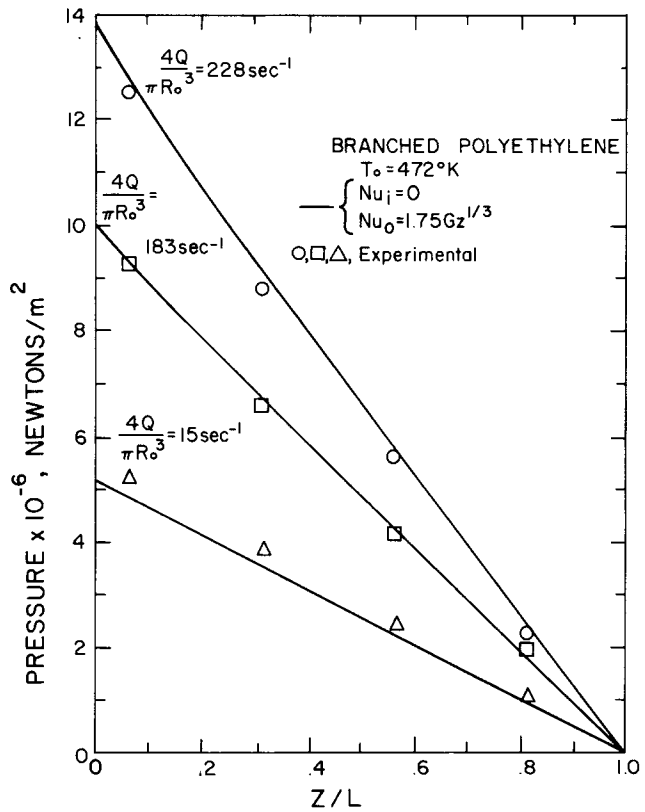

Fig. 17. Axial pressure distribution—annular flow.

TABLE 4. EFFECT OF COMPRESSIBILITY AND EXPANSION

	Exper.	Case 1	Case 2	Case 3
$\Delta P \times 10^{-7}$, N/m²	1.34	1.363	1.371	1.370
ΔT_{Ri}, °K	—	55.79	54.06	53.47
ΔT_{R0}, °K	26	30.19	29.11	28.79
ΔT_b, °K	12	6.26	4.25	4.28

Inner wall adiabatic
Outer wall $Nu_0 = 1.75\ Gz^{1/3}$
$T_0 = 472$°K
$\frac{4Q}{\pi R_0^3} = 228\ s^{-1}$

1. No effect of compressibility or expansion
   $\rho = \rho_0$
   $\epsilon = 0$
2. Effect of expansion only in energy equation
   $\rho = \rho_0$
   $\epsilon = \epsilon_0 = 6.32 \times 10^{-4}\ °K^{-1}$
3. Effect of compression and expansion
   $\rho = \rho(T, P)$
   $\epsilon = -\frac{1}{\rho}\left(\frac{\partial \rho}{\partial T}\right)_p$

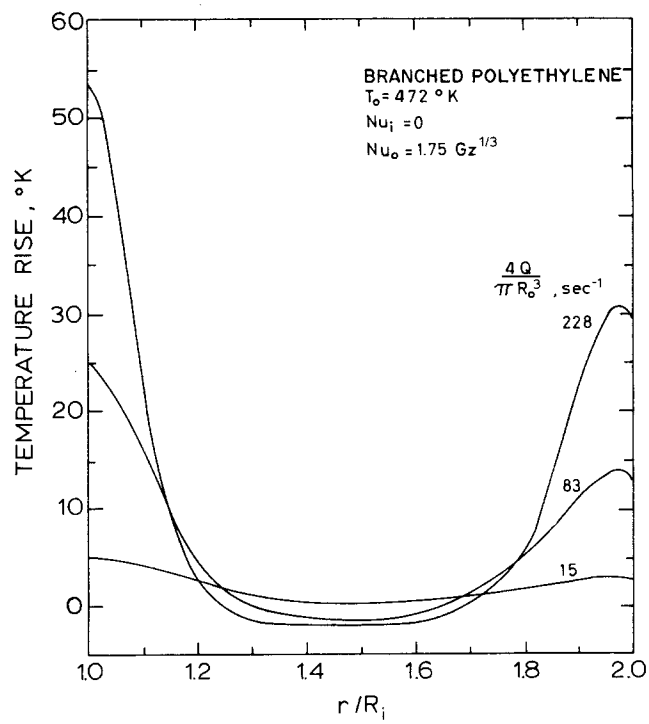

Fig. 18. Temperature profiles at annular exit.

calculations using

$$\eta = \eta_{atm}\, e^{bp}$$

show less than a 4% change in the calculated shear stress and an even smaller change in the surface temperature rise. A value of $b = 4.35 \times 10^{-9}$ m²/N as reported by Duvdevani and Klein (1967) for polyethylene was used for calculations. Any increase of viscosity with pressure results in a shear stress and temperature rise greater than those calculated with no pressure dependence. Recalling Figures 5, 7, and 13, an adiabatic wall with no pressure dependence yields calculated temperature rises much larger than the measured temperature rises. This supports the conclusion that neither an adiabatic nor an isothermal wall exists.

Summary

Temperature profiles are needed to further confirm the

model. They would allow a much better method of determining the type of boundary condition present. Noncontact methods are necessary because common methods such as thermocouple probes can give misleading measurements due to disruption of the flow and shear heating at the thermocouple surface.

A possible method to obtain some knowledge of the internal temperature of the melt might be to utilize some of the optical properties of polymer (for example, index of refraction) in conjunction with the transparent character of most pure polymer melts (for example, polystyrene and polyethylene).

The knowledge of temperature profiles would allow the importance of thermal expansion to be evaluated. As was mentioned earlier, thermal expansion has the greatest effect on the temperature profile in the center of the die.

It is expected that some polymer degradation occurs due to the large temperature rises and shear rates encountered. While degradation may not seriously affect design quantities such as pressure drop, certain characteristics of the product such as the surface finish may be adversely affected by the high temperatures encountered near the surface. Shear heating has generally not been considered in degradation studies [see Casale et al. (1971) for a recent review].

ACKNOWLEDGMENT

The authors would like to thank Union Carbide for financial support, Uniroyal and Marbon for materials, and Western Electric Co. for permission to publish some of the experimental data.

NOTATION

a_T = temperature shift factor defined by Equation (6)
a_1-a_6 = parameters in Equation (7)
a_7-a_9 = parameters in Equation (8)
b = width of slit, cm
c_1-c_2 = parameters in Equation (6)
c_l = parameter in Equation (4)
c_p = heat capacity, J/kg · °K
d = depth of slit, cm
h = heat transfer coefficient, W/m² · °K
k = thermal conductivity, W/m · °K
L = length of slit, capillary, or annulus, cm
m = parameter in Equation (4)
P = pressure, N/m²
P' = dimensionless pressure
$= P\left(\frac{d^2}{4\eta_0{}^0\,\bar{v}\,L}\right)$ slit
Q = volumetric flow rate, cm³/s
r = radial distance variable, cm
R = capillary radius, cm
R_i = inner radius of annulus, cm
R_o = outer radius of annulus, cm
T = temperature, °K
T_b = bulk temperature, °K
T_0 = inlet and die temperature, °K
T' = dimensionless temperature
$= T/T_0$
v_z = axial velocity, cm/s
v'_z = dimensionless axial velocity
$= v_z/\bar{v}$
v_y = velocity in y coordinate direction, cm/s
v'_y = dimensionless velocity
$= v_y/\bar{v}$
$\bar{v}$ = characteristic velocity
y = coordinate direction, cm
y' = dimensionless coordinate direction
$= 2y/d$
z = axial distance variable, cm
z' = dimensionless axial distance
$= z/L$

Greek Letters

β = R_o/R_i
$\dot{\gamma}$ = shear rate, s^{-1}
$\dot{\gamma}_a$ = apparent shear rate, s^{-1}
$= 32Q/\pi D^3$ capillary
$= 6Q/bd^2$ slit
ϵ = coefficient of thermal expansion, °K^{-1}
$= -\frac{1}{\rho}\left(\frac{\partial\rho}{\partial T}\right)_p$
ϵ' = dimensionless ϵ
$= \epsilon T_0$
η = melt viscosity, N s/m²
η_r = zero shear viscosity at reference temperature T_r, N s/m²
η_0 = zero shear viscosity, N s/m²
$\eta_0{}^0$ = zero shear viscosity at $T = T_0$, N s/m²
η' = dimensionless viscosity
$= \eta/\eta_0{}^0$
ρ = density, kg/m³
ρ_0 = density at $T = T_0$, $P = 0$
ρ' = dimensionless density
$= \rho/\rho_0$
τ_{yz} = shear stress, N/m² slit
τ'_{yz} = dimensionless shear stress
$= \left(\frac{d^2}{4\eta_0{}^0\,v\,L}\right)\tau_{yz}$
τ_w = apparent shear stress at wall
$= \frac{\Delta P}{2L/R}$ capillary
$= \frac{\Delta P}{2L/d}$ slit

Dimensionless Groups

Pr = $\eta_0{}^0 c_p/k$
Re = $\bar{v}\,d\rho_0/\eta_0{}^0$
Gz = wc_p/kL
Nu = $2hR/k$ capillary
$= hd/k$ slit
Nu_i = $2h_iR_i/k$
Nu_0 = $2h_0R_0/k$
Br = $\frac{\eta_0{}^0\,\bar{v}^2}{kT_0}$

Subscripts

i = inner wall of annulus
o = outer wall of annulus
r = reference

LITERATURE CITED

Bagley, E. B., "End Corrections in the Capillary Flow of Polyethylene," *J. Appl. Phys.*, **28**, 624 (1957).

Bergen, R. L., and H. L. Morris, "The Melt Rheology of ABS Polymers," *Proc. 5th Intern. Congr. on Rheol.*, Univ. of Tokyo Press (1970).

Bird, R. B., "Viscous Heat Effects in Extrusion of Molten Plastics," *SPE J.*, **11**, 35 (1955).

Brinkman, H. C., "Heat Effects in Capillary Flow," *Appl. Sci. Res.*, A2, 120 (1951).

Casale, A., R. S. Porter, and J. F. Johnson, "The Mechanochemistry of High Polymers," *Rubber Chem. Tech.*, **44**, 534 (1971).

Cox, H. W., Ph.D. thesis, Univ. Minnesota, Minneapolis (1973).

———., and C. W. Macosko, "The Effect of Shear Heating

on Capillary Flow," *SPE ANTEC*, **20**, 28 (1974).
Donovan, R. C., "A Theoretical Melting Model for Plasticating Extruders," *Polym. Eng. Sci.*, **11**, 247 (1971).
Duvdevani, I. J., and I. Klein, "Analysis of Polymer Melt Flow in Capillaries Including Pressure Effects," *SPE J.*, **23**(12), 41 (1967).
Galili, N., and R. Takserman-Krozer, "Heat Effect in Viscous Flow through a Pipe," *Israel J. Tech.*, **9**, 439 (1971).
Gillespie, T., "The Flow of a Molten Polymer," *Trans. Soc. Rheol.*, **9**, 35 (1965).
Gee, R. E., and J. B. Lyon, "Non-Isothermal Flow of Viscous Non-Newtonian Fluids," *Ind. Eng. Chem. Fundamentals*, **49**, 956 (1957).
Gerrard, J. E., R. E. Steidler, and J. K. Appeldoorn, "Viscous Heating in Capillaries: The Adiabatic Case," *Ind. Eng. Chem. Fundamentals*, **4**, 332 (1965).
———., "Viscous Heating in Capillaries: The Isothermal-Wall Case," *ibid.*, **5**, 260 (1966).
Kim, H. T., and E. A. Collins, "Temperature Profiles for Polymer Melts in Tube Flow. II. Conduction and Shear Heating Corrections," *Polym. Eng. Sci.*, **11**, 83 (1971).
Macosko, C. W., "Determination of Polymer Viscosities at Processing Conditions," Western Electric Co. Report (Jan., 1970).
———., and J. R. Starita, "New Rheometer is Put to the Test," *SPE J.*, **27**(11), 38 (1971).
Marshall, D. E., I. Klein, and R. H. Uhl, "Measurement of Screw and Plastic Temperature Profiles in Extruders," *ibid.*, **20**, 329 (1964).
Merz, E. H., and R. E. Colwell, "A High Shear Rate Capillary Rheometer for Polymer Melts," *ASTM Bull.*, **232**, 63 (Sept., 1958).
Middleman, S., *The Flow of High Polymers*, Interscience, New York (1968).
Morrette, R. A., and C. G. Gogos, "Viscous Dissipation in Capillary Flow of Rigid PVC and PVC Degradation," *Polym. Eng. Sci.*, **8**, 272 (1968).
Pearson, J. R. A., *Mechanical Properties of Polymer Melt Processing*, Pergamon Press, Oxford (1966).
Propper, G. A., and R. C. Donovan, "The Viscometric Flow of Polymer Melts in Annular Flow," Western Electric Co. Report, (1971).
Toor, H. L., "The Energy Equations for Viscous Flow-Effect of Expansion on Temperature Profiles," *Ind. Eng. Chem. Process Design Develop.* **48**, 922 (1956).
———., "Heat Generation and Conduction in the Flow of a Viscous Compressible Liquid," *Trans. Soc. Rheol.*, **1**, 177 (1957).
Van Leeuwen, J., "Stock Temperature Measurement in Plastifying Equipment," *Polym. Eng. Sci.*, **7**, 98 (1967).
Van Ness, R. T., "IR Thermometers to Measure PE Melt In-Process," *Plast. Tech.*, **11**, (Dec., 1965).
Rogers, C. E., W. I. Vroom, and R. F. Westover, "Getting the Most from Polymers by Vacuum Compression Mold," *Mod. Plast.*, 200 (Sept., 1968).

APPENDIX

With primes denoting dimensionless quantities, Equations (1) to (3) can be written

$$\frac{\partial}{\partial z'}(\rho' v'_z) + \frac{2L}{d}\frac{\partial}{\partial y'}(\rho' v'_y) = 0 \tag{A1}$$

$$0 = -\frac{dP'}{dz'} - \frac{2L}{d}\frac{\partial \tau'_{yz}}{\partial y'} \tag{A2}$$

$$\frac{RePr}{4L/d}\left(\rho' v'_z \frac{\partial T'}{\partial z'} + \frac{2L}{d}\rho' v'_y \frac{\partial T'}{\partial y'}\right) = \frac{\partial^2 T'}{\partial y'^2} - \frac{2L}{d} Br \tau'_{yz}\frac{\partial v'_z}{\partial y'} + BrT'\epsilon' v'_z \frac{dP'}{dz'} \tag{A3}$$

with boundary conditions

$$\frac{\partial T'}{\partial y'} = 0 \qquad y' = 0,\ 0 < z' < 1$$

$$\tau'_{yz} = 0 \qquad y' = 0,\ 0 < z' < 1$$

$$v'_z = v'_y = 0 \qquad y' = 1,\ 0 < z' < 1$$

$$\frac{\partial T'}{\partial y'} = Nu(1 - T') \qquad y' = 1,\ 0 < z' < 1$$

$$T' = 1 \qquad z' = 0,\ 0 < y' < 1$$

$$v'_z = v'_{z0}(y') \qquad z' = 0,\ 0 < y' < 1$$

$$v'_y = 0 \qquad z' = 0,\ 0 < y' < 1$$

$$P' = 0 \qquad z' = 1,\ 0 < y' < 1$$

Equation (A3) is highly nonlinear in that the coefficients of the differential operators $\left(\rho',\ v'_z,\ v'_y,\ \eta',\ \frac{\partial P'}{\partial z'},\ \tau'_{yz}\right)$ are functions of temperature, either directly (ρ', η') or indirectly through the viscosity $\left(v'_z,\ v'_y,\ \frac{dP'}{dz'},\ \tau'_{yz}\right)$. However, the use of an iteration procedure results in a linear equation with nonconstant coefficients which can be readily solved by difference methods.

Equation (A3) may be written as

$$\frac{RePr}{4L/d}\left[(\rho' v'_z)^k\left(\frac{\partial T'}{\partial z'}\right)^{k+1} + \frac{2L}{d}(\rho' v'_y)^k\left(\frac{\partial T'}{\partial y'}\right)^{k+1}\right] = \left(\frac{\partial^2 T'}{\partial y'^2}\right)^{k+1} - \frac{2L}{d} Br\left(\tau'_{yz}\frac{\partial v'_z}{\partial y'}\right)^k + BrT'^{k+1}\left(\epsilon' v'_z \frac{dP'}{dz'}\right)^k \tag{A4}$$

where k is an iteration parameter. If the temperature is known for the kth iteration at all points in the space of the die (that is, $0 \leq y' \leq 1$, $0 \leq z' \leq 1$), estimates of the coefficients at all points in the space of the die can be obtained in the following manner:

Noting that

$$\tau'_{yz} = -\frac{d}{2L}\eta'\frac{\partial v'_z}{\partial y'} \tag{A5}$$

Equation (A2) gives, after integration with respect to y'

$$v'_z(y', z') = \frac{dP'}{dz'}\int_1^{y'} \frac{\bar{y}\, d\bar{y}}{\eta'} \tag{A6}$$

An integrated form of the continuity equation yields another condition. This form states that the mass flow rate must be constant at any axial position in the die. In dimensionless form, this statement may be expressed as

$$\int_0^1 \rho' v'_z dy' = 1 \tag{A7}$$

Combining Equations (A6) and (A7), the pressure gradient may be determined by

$$\frac{dP'}{dz'}(z') = \left[\int_0^1 \rho' \int_1^{y'} \frac{\bar{y}\, d\bar{y}}{\eta'} dy'\right]^{-1} \tag{A8}$$

Equation (A1) can be solved to give the y component of velocity as a function of the axial velocity:

$$v'_y(y', z') = -\frac{d}{2L\rho'}\int_1^{y'} \frac{\partial}{\partial z'}(\rho' v'_z)\, d\bar{y} \tag{A9}$$

Thus, Equation (A4) is a linear equation in T'^{k+1} with nonconstant coefficients given by Equations (A5) to (A9). Equation (A4) can be readily solved by difference methods to obtain T'^{k+1} at all points in the space of the die. New estimates of the coefficients are then obtained from Equations (A5) to (A9) and the equation for T'^{k+2} is solved. This pro-

cedure is repeated until the temperatures for two successive iterations agree to within a specified tolerance at all points in the space of the die. The procedure is started by assuming the entire die is at the inlet temperature T_0.

Fully developed non-Newtonian isothermal flow was assumed to exist at the die inlet. That is, $v'_{z0}(y')$ is the solution to Equations (A6) and (A8) at $T = T_0$. $v'_{z0}(y')$ was not calculated separately, but was determined along with the overall solution of $T'(r', z')$, $v'_z(r', z')$, etc. by the procedure explained above.

Three point implicit central difference approximations were used in the y direction while two point backward differences were used in the z direction. Large temperature gradients are encountered near the tube walls and near the inlet. Thus, a finer grid was used in those regions to facilitate convergence of the numerical solution. Some details of the numerical solution and a listing of the program used here are given by Cox (1973).

Manuscript received October 29, 1973; revision received April 2 and April 5, 1974.

Kinetics of Ice Crystallization in Sugar Solutions and Fruit Juices

Ice-crystal secondary nucleation kinetics are derived from thermal response experiments carried out with concentrated sugar solutions and fruit juices. Variables studied include the level of supersaturation, power input, sugar concentration, sugar type, and the presence of high-molecular-weight additives. The nucleation rate is indicated to have a low-order dependence upon subcooling (about 1.25 power) for subcoolings in the range 0.25 to 1.00°C. Fruit juices are well modeled by the corresponding synthetic sugar solution. The selection and improvement of processing approaches for freeze concentration of food liquids are discussed in light of the experimental results.

A. MONEM OMRAN
and
C. JUDSON KING

Department of Chemical Engineering
University of California
Berkeley, California 94720

SCOPE

Freeze concentration is attractive as a means of removing water from food liquids because of the high selectivity of water incorporation into ice, because of the relatively mild processing conditions involved, and because there need not be an opportunity for the loss of volatile flavor and aroma components. Freeze concentration has been limited in application because of the economic penalty associated with loss of concentrate entrained with the ice crystals. This loss can be reduced if a larger average ice crystal size can be obtained. Ice-crystal size, in turn, is determined by relative nucleation and growth kinetics. Nucleation under typical conditions for freeze concentration is dominated by secondary nucleation.

Rates of secondary nucleation as affected by variables other than parent crystal size and density were measured from the duration of the induction period of the thermal response following seeding, under the assumption of diffusion-limited growth. Both sugar solutions and real fruit juices were examined. The results so obtained were then utilized for considerations of preferred and improved design approaches for freeze concentrators.

CONCLUSIONS AND SIGNIFICANCE

Ice secondary nucleation rates, as derived from the induction period of the thermal response, were found to vary as the 1.25 power of subcooling for temperature subcoolings in the range 0.25 to 1.00°C. The nucleation rate increases with increasing power input to the system and increases markedly with increasing sugar concentration, but is relatively independent of sugar type. The nucleation rate was also found to be suppressed by the addition of pectin or gelatin. Orange and apple juice are modeled reasonably well by the corresponding synthetic sugar solution. The transient portion of the response can be used to infer that ice-crystal growth rates are governed by established correlations for turbulent mass transfer to suspended particles, provided that the transient response is assumed to be dominated by a fixed number of crystals of largest size. Further research is required to establish the extent to which new nuclei themselves become sources of secondary nucleation.

For the nucleation kinetics found in this subcooling range the crystal-size distribution will not change much with changing subcooling for a given ice production. The decrease of ice crystal size with sugar content discourages the use of recycle as a means of building up the volume fraction of liquid in a freeze concentration process. Benefits achievable by appropriate staging of the freezing process are explored.

Correspondence concerning this paper should be addressed to C. J. King. A. M. Omran is with D. E. J. International Research Co. B. V., Utrecht, Netherlands.